

<sup>1</sup> **Whole-brain comparison of rodent and human brains  
using spatial transcriptomics**

<sup>3</sup>

<sup>4</sup> Antoine Beauchamp<sup>1,2,3,\*</sup>, Yohan Yee<sup>1,2,3</sup>, Ben C. Darwin<sup>1,2</sup>, Armin Raznahan<sup>4</sup>, Rogier B.  
<sup>5</sup> Mars<sup>5,6,†</sup>, Jason P. Lerch<sup>1,2,3,5,\*†</sup>

<sup>6</sup>

<sup>7</sup> <sup>1</sup>Mouse Imaging Centre, Toronto, Ontario, Canada.

<sup>8</sup> <sup>2</sup>The Hospital for Sick Children, Toronto, Ontario, Canada.

<sup>9</sup> <sup>3</sup>Department of Medical Biophysics, University of Toronto, Toronto, Ontario, Canada.

<sup>10</sup> <sup>4</sup>Section on Developmental Neurogenomics, Human Genetics Branch, National Institute of Mental Health Intramural  
<sup>11</sup> Research Program, Bethesda, MD, U.S.A.

<sup>12</sup> <sup>5</sup>Wellcome Centre for Integrative Neuroimaging, Centre for Functional MRI of the Brain (FMRIB), Nuffield Depart-  
<sup>13</sup> ment of Clinical Neurosciences, John Radcliffe Hospital, University of Oxford, Oxford, United Kingdom.

<sup>14</sup> <sup>6</sup>Donders Institute for Brain, Cognition and Behaviour, Radboud University Nijmegen, Nijmegen, Netherlands.

<sup>15</sup> <sup>†</sup>These authors contributed equally to this work.

<sup>16</sup> \*Corresponding author. Email: antoine.beauchamp@mail.utoronto.ca (A.B.); jason.lerch@ndcn.ox.ac.uk (J.P.L)

<sup>17</sup> **Abstract**

<sup>18</sup> The ever-increasing use of mouse models in preclinical neuroscience research calls for an improvement in the  
<sup>19</sup> methods used to translate findings between mouse and human brains. Previously we showed that the brains  
<sup>20</sup> of primates can be compared in a direct quantitative manner using a common reference space built from  
<sup>21</sup> white matter tractography data (Rogier B. Mars et al., 2018b). Here we extend the common space approach  
<sup>22</sup> to evaluate the similarity of mouse and human brain regions using openly accessible brain-wide transcrip-  
<sup>23</sup> tomic data sets. We show that mouse-human homologous genes capture broad patterns of neuroanatomical  
<sup>24</sup> organization, but that the resolution of cross-species correspondences can be improved using a novel su-  
<sup>25</sup> pervised machine learning approach. Using this method, we demonstrate that sensorimotor subdivisions of  
<sup>26</sup> the neocortex exhibit greater similarity between species, compared with supramodal subdivisions, and that  
<sup>27</sup> mouse isocortical regions separate into sensorimotor and supramodal clusters based on their similarity to  
<sup>28</sup> human cortical regions. We also find that mouse and human striatal regions are strongly conserved, with  
<sup>29</sup> the mouse caudoputamen exhibiting an equal degree of similarity to both the human caudate and putamen.

## 30 Introduction

31 Animal models play an indispensable role in neuroscience research, not only for understanding disease and  
32 developing treatments, but also for obtaining data that cannot be obtained in the human. While numerous  
33 species have been used to model the human brain, the mouse has emerged as the most prominent of these,  
34 due to its rapid life cycle, straightforward husbandry, and amenability to genetic engineering (Dietrich et  
35 al., 2014; Ellenbroek and Youn, 2016; Hedrich et al., 2004; Houdebine, 2004). Mouse models have proven  
36 to be extremely useful for understanding diverse features of the brain, from its molecular neurobiological  
37 properties to its large-scale network properties (Hodge et al., 2019; Oh et al., 2014; Yao et al., 2021).  
38 However, translating findings from the mouse to the human has not been straightforward. This is especially  
39 evident in the context of neuropsychopharmacology, where promising neuropsychiatric drugs have one of the  
40 highest failures rates in Phase III clinical trials (Hay et al., 2014).

41 Successful translation requires an understanding of how effects on the brain of the model species are likely to  
42 manifest in the brain of the actual species of interest. This is not trivial in the case of the mouse and human,  
43 as the two species diverged from a common ancestor about 80 million years ago (Kaas, 2012). Although  
44 common themes are apparent in the brains of all mammalian species studied to date (Krubitzer, 2007), there  
45 remain substantial differences between the mouse and human brain. Beyond the obvious differences in size,  
46 large parts of the human cortex potentially have no corresponding homologues in the mouse (Preuss, 1995).  
47 Direct comparisons across the brains of different species are further complicated by the fact that researchers  
48 from different traditions use inconsistent nomenclature to refer to similar neuroanatomical areas (Heukelum  
49 et al., 2020; Laubach et al., 2018).

50 Over the course of the last decade, we have developed novel approaches to explicitly evaluate similarities  
51 and differences between the brains of related species. These approaches describe brains using common data  
52 spaces that are directly comparable between species, making it possible to evaluate the similarity of different  
53 regions in a quantitative fashion (Mars et al., 2021). This way, potential homologues can be formally tested  
54 and regions of the brain that do not allow for straightforward translation can be identified (Rogier B. Mars  
55 et al., 2018b). Establishing such a formal translation between the mouse and the human brain would allow  
56 scientists involved in translational research to explicitly test hypotheses about conservation of brain regions,  
57 identify regions that are well suited to translational paradigms, and directly transform quantitative maps  
58 from the brain of one species to the other.

59 One approach towards building these common spaces has been to exploit connectivity. The connections of  
60 a brain region tend to be unique and can therefore be seen as a diagnostic of an area (Rogier B. Mars et

al., 2018a; Passingham et al., 2002). The common connectivity space approach relies on defining agreed upon neuroanatomical homologues a priori and then expressing the connectivity fingerprint of regions under investigation with those established homologues in the two brains (Mars et al., 2016b). The connections of any given region to the established homologues thus form a common space, which links the two brains. In a series of early studies, we compared the connectivity of the macaque and human brain, identifying homologies as well as specializations across association cortex (Mars et al., 2013; Neubert et al., 2014; Sallet et al., 2013). The same approach has recently been applied to mouse-human comparisons for the first time, demonstrating conserved organization between the mouse and human striatum, but some specialization in the human caudate related to connectivity with the prefrontal cortex (Balsters et al., 2020). A similar study recently compared connectivity of the medial frontal cortex across rats, marmosets, and humans (Schaeffer et al., 2020). However, the lack of established neuroanatomical homologues in mice, particularly in the cortex, limits the use of connectivity to compare these species.

A more promising approach to mouse-human comparisons could be to exploit the spatial patterns of gene expression. Advances in transcriptomic mapping can be used to characterise the differential expression of many thousands of genes across the brain and compare the pattern between regions (Ortiz et al., 2020). Moreover, the availability of whole-brain spatial transcriptomic data sets for multiple species provides an opportunity to run novel analyses at low cost (Hawrylycz et al., 2012; Lein et al., 2007). Such maps for the human cortex show topographic patterns that mimic those observed in other modalities, such as a gradient between primary and heteromodal areas of the neocortex (Burt et al., 2018). Importantly, these patterns appear to be conserved across mammalian species (Fulcher et al., 2019), which opens up the possibility of using the expression of homologous genes as a common space across species. In fact, a recent study demonstrated how the expression of homologous genes can be used to directly register mouse and vole brains into a common reference frame, which allows for direct point-by-point comparisons of brain maps (Englund et al., 2021). However, this specific approach is only feasible because of the large degree of morphological similarity between mouse and vole brains. In the case of mouse-human comparisons, we almost certainly cannot directly register mouse and human brains into a common coordinate frame using methods for image registration. Hence we need to be more creative in our approach.

Here we examine the patterns of similarity between the mouse and human brain using a common space constructed from spatial gene expression data sets. We begin with an initial set of 2624 homologous genes. Subsequently, we present and evaluate a novel method for improving the resolution of mouse-human neuroanatomical correspondences using a supervised machine learning approach. Using the novel representation of the gene expression common space, i.e. a latent gene expression space, we analyse the similarity of mouse

93 and human isocortical subdivisions and demonstrate that sensorimotor regions exhibit a higher degree of sim-  
94 ilarity than supramodal regions. Finally, we examine the patterns of transcriptomic similarity at a voxel-wise  
95 level in the mouse and human striatum.

## 96 Results

### 97 Homologous genes capture broad similarities in the mouse and human brains

98 We first examined the pattern of similarities that emerged when comparing mouse and human brain regions  
99 on the basis of their gene expression profiles. We constructed a gene expression common space using widely  
100 available data sets from the Allen Institute for Brain Science: the Allen Mouse Brain Atlas (AMBA) and  
101 the Allen Human Brain Atlas (AHBA) (Hawrylycz et al., 2012; Lein et al., 2007). These data sets provide  
102 whole-brain coverage of expression intensity for thousands of genes in the mouse and human genomes.  
103 For our purposes we filtered these gene sets to retain only mouse-human homologous genes using a list  
104 of orthologues obtained from the NCBI HomoloGene system (NCBI 2018). Prior to analysis, both data  
105 sets were pre-processed using a pipeline that included quality control checks, normalization procedures, and  
106 aggregation of the expression values under a set of atlas labels. The result was a gene-by-region matrix in  
107 either species, describing the normalized expression of 2624 homologous genes across 67 mouse regions and  
108 88 human regions (see Materials and methods). We quantified the degree of similarity between all pairs of  
109 mouse and human regions using the Pearson correlation coefficient, resulting in a mouse-human similarity  
110 matrix (Fig. 1A).

111 We find that the similarity matrix exhibits broad patterns of positive correlation between the mouse and  
112 human brains. These clusters of similarity correspond to coarse neuroanatomical regions that are generally  
113 well-defined in both species. For instance, we observe that, overall, the mouse isocortex is similar to the  
114 human cerebral cortex, with the exception of the hippocampal formation, which forms a unique cluster.  
115 Similarly the mouse and human cerebellar hemispheres cluster together, while the cerebellar nuclei show  
116 relatively high correlation to each other ( $r = 0.404$ ) as well as to brain stem structures like the pons ( $r = 0.359$ )  
117 and  $r = 0.371$  for the mouse and human nuclei respectively) and myelencephalon ( $r = 0.318$  and  $r = 0.374$ ).  
118 The associations between broad regions such as these are self-evident in the correlation matrix.

119 Our ability to resolve regional matches on a finer scale is limited when using all homologous genes in this way.  
120 This is especially true for regions within the cerebral and cerebellar cortices, which exhibit a high degree  
121 of internal homogeneity. This is apparent in the similarity profiles, defined here as the set of correlation

122 values between a given seed region and all target regions in the other species. For example, the human  
123 precentral gyrus and cuneus are most strongly correlated to many regions of the mouse isocortex. While  
124 the brain maps feature a rostral-caudal gradient (Fig. 1B), the profiles of the two seeds are highly similar  
125 despite the regions having very different functions (Fig. 1C). Indeed, the correlation between the similarity  
126 profiles of the precentral gyrus and cuneus is  $r = 0.980$ . The similarity profile of human cerebellar crus 1  
127 highlights another example of this homogeneity. The profile of crus 1 is similar to that of all regions of the  
128 mouse cerebellum, with an average correlation of  $r = 0.269$  and a standard deviation of  $\sigma = 0.041$ . Across  
129 all regions, the variance of the correlations across cortical regions is  $\sigma^2 = 0.0052$  while that across cerebellar  
130 hemispheric regions is  $\sigma^2 = 0.0017$ , compared with a total variation of  $\sigma^2 = 0.0416$  across all entries in the  
131 matrix.

132 So, although there is some distinguishing power in the profiles of regions at a finer scale, this is much smaller  
133 than between coarse anatomical regions. This is also true for parts of the broad anatomical systems that are  
134 part of the same functional system. This suggests that the regional expression patterns of mouse-human  
135 homologous genes can be used to identify general similarities between the brains of the two species even  
136 using a simple correlation measure, but the ability to identify finer scale matches might require a more  
137 subtle approach.

### 138 **A latent gene expression space improves the resolution of mouse-human associations**

139

140 In the previous analyses, we showed that the expression profiles of homologous genes capture broad simi-  
141 larities across the mouse and the human for the major subdivisions of the brain. Some information at a  
142 finer resolution (e.g. within the isocortex) was also evident, but much less distinctive. Our next goal was  
143 to investigate whether it is possible to leverage the gene expression data sets to relate mouse and human  
144 brains to one another at a finer regional level. In order to do so, we sought to maximise the informational  
145 value in the set of 2624 homologous genes by creating a new latent common space that exploits the regional  
146 distinctiveness of the expression profiles.

147 The approach used in the previous analysis relied on using homologous genes as a common space between  
148 the mouse and human brain. This approach effectively assigns equal value to each gene, whereas a more  
149 powerful approach would be to weight genes by their ability to distinguish between different brain regions.  
150 We investigated whether we could accomplish this by constructing a new set of variables from combinations  
151 of the homologous genes. Our primary goal here was to transform the initial gene space into a new common

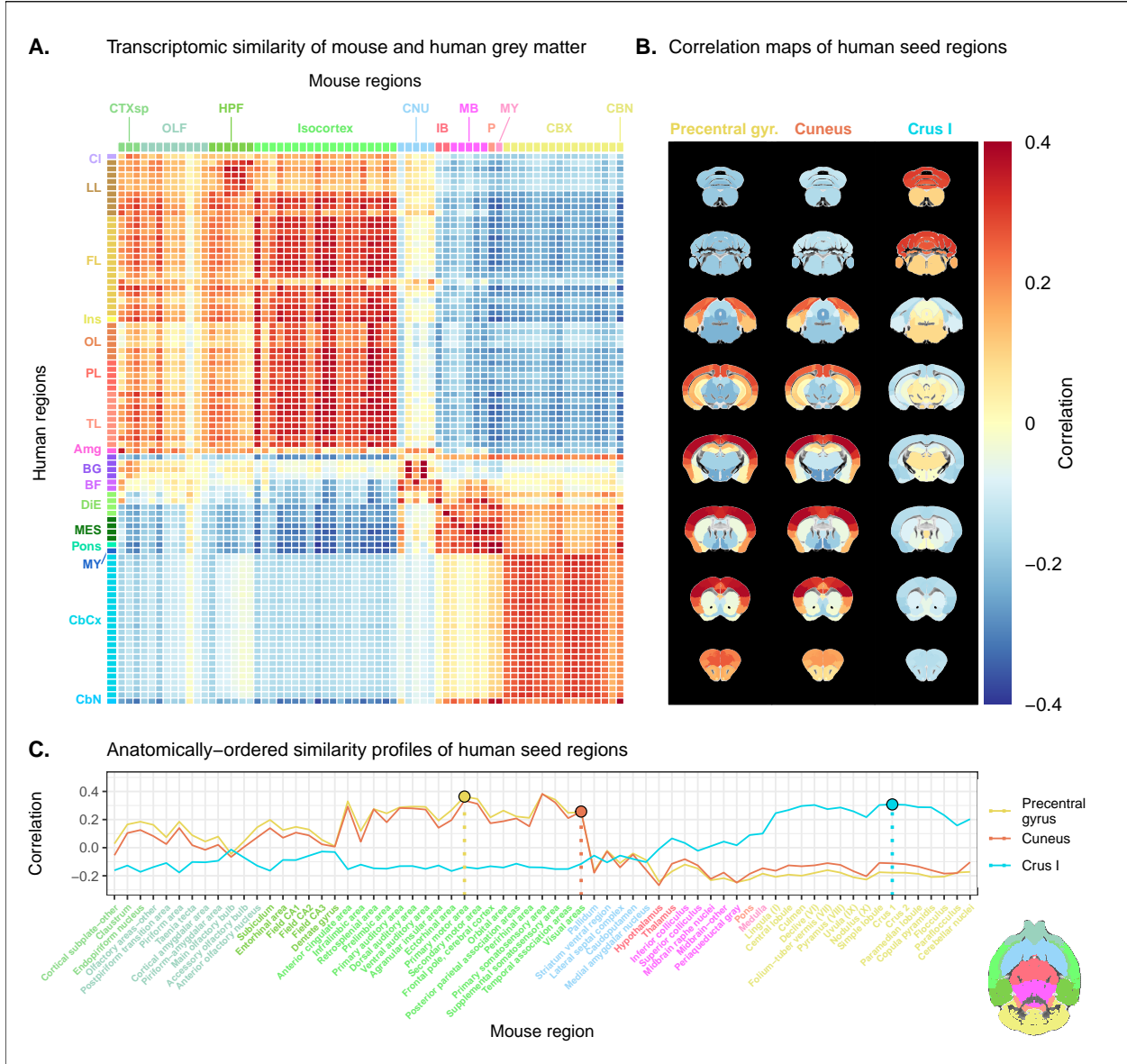


**Fig. 1. Transcriptomic similarity in the mouse and human brains.** (A) Similarity matrix displaying the correlation between 67 mouse regions and 88 human regions based on the expression of 2624 homologous genes. Columns are annotated with 11 broad mouse regions: Cortical subplate (CTXsp), olfactory areas (OLF), hippocampal formation (HPF), isocortex, cerebral nuclei (CNU), interbrain (IB), midbrain (MB), pons (P), medulla (MY), cerebellar cortex (CBX), cerebellar nuclei (CBN). Rows are annotated with 16 broad human regions: Claustrum (Cl), limbic lobe (LL), frontal lobe (FL), insula (Ins), occipital lobe (OL), parietal lobe (PL), temporal lobe (TL), amygdala (Amg), basal ganglia (BG), basal forebrain (BF), diencephalon (DIE), mesencephalon (MES), pons, myelencephalon (MY), cerebellar cortex (CbCx), cerebellar nuclei (CbN). Broad patterns of similarity are evident between coarsely defined brain regions, while correlation patterns are mostly homogeneous within these regions. (B) Mouse brain coronal slices showing similarity profiles for the human precentral gyrus, cuneus and crus I. Correlation patterns for the precentral gyrus and cuneus are highly similar to one another and broadly similar to most isocortical regions. The crus I is homogeneously similar to the mouse cerebellum. (C) Anatomically-ordered line charts displaying the similarity profiles for the seed regions in (B). Dashed vertical lines indicate the canonical mouse homologue for each human region. Annotation colours correspond to atlas colours from the AMBA and AHBA for mouse and human respectively.

space that would improve the locality of the matches. However while we sought a transformation that would allow us to recapitulate known mouse-human neuroanatomical homologues, we also wanted to avoid directly encoding such correspondences in the transformation. Using this information as part of the optimization process for the transformation would run the risk of driving the transformation towards mouse-human pairs that are already known. While we are interested in being able to recover such matches, we are equally interested in identifying novel and unexpected associations between neuroanatomical regions in the mouse and human brains (e.g. one-to-many correspondences). Given these criteria, our approach to identifying an appropriate transformation was to train a multi-layer perceptron classifier on the data from the AMBA. The classifier was tasked with predicting the 67 labels in our mouse atlas from the voxel-wise expression of the homologous genes (Fig. 2A).

While the model could have been trained using the data from either species, we chose to use the mouse data because it provides continuous coverage of the entire brain and is thus better suited to this purpose. In training the model to perform this classification task, we effectively optimize the network architecture to identify a transformation from the input gene space to a space that encodes information about the delineation between mouse brain regions. To extract this transformation, we removed the output layer from the trained neural network. The resulting architecture defines a transformation from the input space to a lower-dimensional gene expression latent space. We then applied this transformation to the mouse and human gene-by-region expression matrices to obtain representations of the data in the latent common space (Fig. 2B). Finally, we used these gene expression latent common space matrices to compute the new similarity matrix (Fig. 2C). Since the optimization algorithm used to train the perceptron features an inherent degree of stochasticity, we repeated this training and transformation process 500 times to generate a distribution of latent spaces and similarity matrices over training runs.

To assess whether the latent space representations of the data improved the resolution of the mouse-human matches, we considered two criteria. The first was whether the similarity profiles of the mouse atlas regions were more localized within the corresponding broad regions of interest (e.g. primary motor area within isocortex), compared with their similarity profiles in the original gene space. We term this the locality criterion. The second criterion was whether the degree of similarity between canonical neuroanatomical homologues improved in this new latent common space. We term this the homology criterion. The locality criterion tells us about our ability to extract finer-scale signal in these profiles, while the homology criterion informs us about our ability to recover expected matches in this finer-scale signal. To evaluate these criteria, we computed ranked similarity profiles for every region in the mouse brain, ordered such that a rank of 1 indicates the most similar human region. In addition, given the difference in absolute value between the

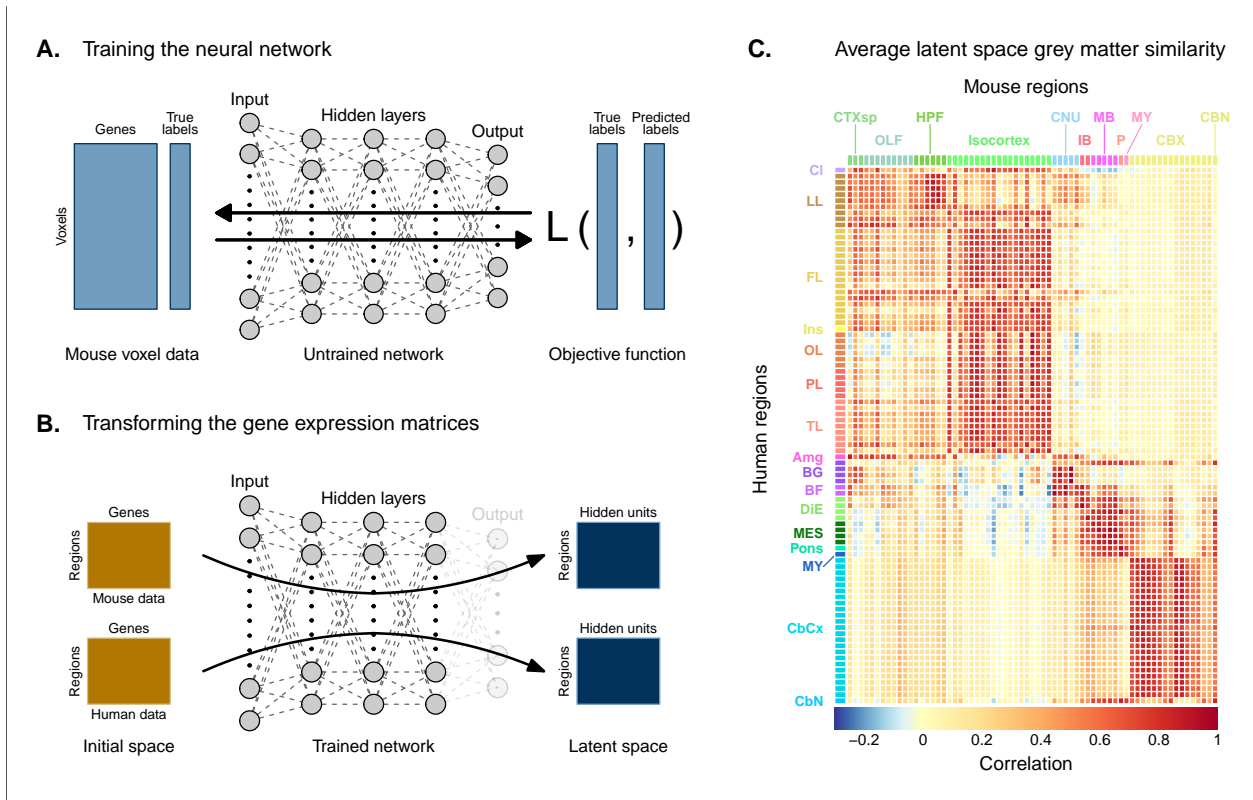


**Fig. 2. Creating a new common space.** (A) Voxel-wise expression maps from 2624 homologous genes in the AMBA were used to train the neural network to classify each mouse voxel into one of 67 atlas regions. (B) Once the network is trained, the output layer is removed. The mouse and human regional gene expression matrices are passed through the network, resulting in lower-dimensional latent space representations of the data. The training and transformation process was repeated 500 times. (C) A similarity matrix displaying the gene expression latent space correlation between mouse and human regions, averaged over 500 neural network training runs. Similar brain regions exhibit very high correlation values. Column and row annotations as described in Figure 1.

184 input gene space and gene expression latent space correlations, we scaled the similarity profiles to the interval  
185  $[0, 1]$  in order to make comparisons between the spaces.

186 We evaluated the locality criterion by examining the decay rate of the top of the similarity profiles. We  
187 reasoned that the plateau of similarity to a broad brain region, as seen in the anatomically-ordered similarity  
188 matrices and profiles (Fig. 1, A and C; Fig. 2C), would correspond to a similar plateau at the head of the  
189 rank-ordered profiles. Moreover, the emergence of local signal would manifest as an increase in the range  
190 between the peaks and troughs within the broad region. In the rank-ordered profiles, this would correspond  
191 to a faster rate of decay at the head of the profile. In order to quantify this decay, we computed the rank  
192 at which each region's similarity profile decreased to a scaled value of 0.75. This was calculated for every  
193 mouse region in the initial gene space, as well as in each of the 500 gene expression latent spaces. As a  
194 measurement of performance between the two representations of the data, we then took the difference in  
195 this rank between each of the latent spaces and the original gene space (Fig. 3A). A negative rank difference  
196 indicates an improvement in the latent space.

197 Examining the structure-wise distributions of these rank differences, we found that for the majority of regions  
198 in our mouse atlas, the classification approach resulted in either an improvement in the amount of locality  
199 within a broad region, or no difference from the original gene space (Fig. 3, B and C). Specifically, 47 regions  
200 (70.1%) had a mean rank difference less than or equal to zero. Additionally, the same number of regions  
201 returned non-positive rank differences in at least 80% of latent spaces. A few regions performed considerably  
202 worse in the latent spaces, notably the main olfactory bulb ( $\mu = 18.4; \sigma = 12.7$ ), the accessory olfactory  
203 bulb ( $\mu = 8.7; \sigma = 11.6$ ), and the cerebellar nuclei ( $\mu = 9.1; \sigma = 8.5$ ). In particular, the main olfactory  
204 bulb performed worse in 96.6% of latent spaces. Regions within the cortical subplate and olfactory areas  
205 (e.g. endopiriform nucleus, postpiriform transition area) benefited the most from the classification approach,  
206 with many regions showing improvements in all latent spaces. While the effects are smaller, the similarity  
207 profiles of regions belonging to the isocortex and cerebellar cortex also saw an improvement in locality. In  
208 the isocortex, 16 out of 19 regions (84.2%) improved in at least 96% of latent spaces. In the cerebellar  
209 cortex, 73.3% of regions saw a similar improvement. In contrast, regions belonging to the cerebral nuclei,  
210 the diencephalon, midbrain and hindbrain did not see much improvement in this new common space. For  
211 instance, only 13.2% of latent spaces returned a non-positive rank difference in the thalamus. For many  
212 such regions the degree of locality appears to be worse in this space, though only by a small number of  
213 ranks (e.g. striatum ventral region, thalamus, midbrain raphe nuclei). Indeed, the mean rank difference  
214 and standard deviation over these regions and all latent spaces are  $\mu = 1.4$  and  $\sigma = 3.6$ . These results  
215 demonstrate that the supervised learning approach used here can improve the resolution of neuroanatomical

correspondences between the mouse and human brains, though the amount of improvement varies over the brain. Regions that were already well-characterized using the initial set of homologous genes (e.g. subcortical regions) did not benefit tremendously, but numerous regions in the cortical plate and subplate, as well as the cerebellum, saw an improvement in locality in this new common space.

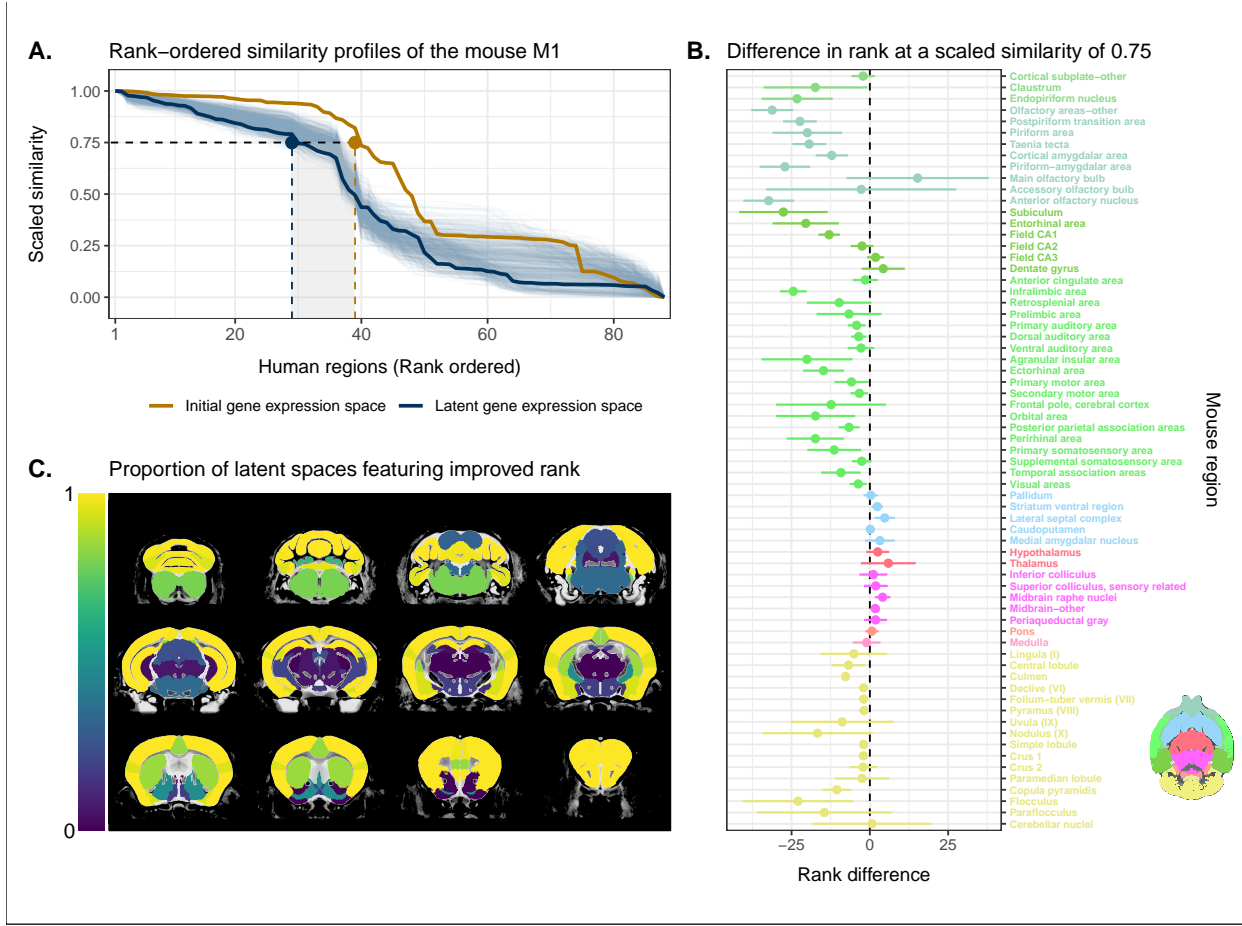


**Fig. 3. Quantifying improvement in locality in gene expression latent space.** (A) The amount of local signal within a broadly similar region of the brain for a finer seed region's (e.g. primary motor area) similarity profile can be quantified by the decay rate of the head of the rank-ordered profile. Decay rate was quantified by computing the rank at a similarity of 0.75. This metric was compared between the initial gene expression space (orange line) and every gene expression latent space resulting from repeated training of the neural network (every blue line is a training outcome, heavy blue line serves as an example). A negative difference between these rank metrics indicates an improvement in locality in the latent space. (B) Structure-wise distributions of differences in rank at a similarity of 0.75 between the initial gene expression space and the gene expression latent spaces. Points and error bars represent mean and 95% confidence interval. Dashed black line at 0 indicates the threshold for improvement in one space over the other. Colours correspond to AMBA annotations as in Figures 1 and 2. (C) Proportion of perceptron training runs resulting in an improvement or null difference in the gene expression latent space compared with the initial space. Cortical and cerebellar regions exhibit high proportions of improvement, while subcortical regions are less likely to be improved by the classification process.

While the supervised learning approach improved our ability to identify matches on a finer scale for a number of brain regions, this does not necessarily mean that those improved matches are biologically meaningful. The second criterion for evaluating the performance of the neural network addresses whether this improvement in locality captures what we would expect in terms of known mouse-human homologies. To this end, we examined the degree of similarity between established mouse-human neuroanatomical pairs, both in the

initial gene expression space and in the set of latent spaces. We began by establishing a list of 36 canonical mouse-human homologous pairs on the basis of common neuroanatomical labels in our atlases. For each of these regions in the mouse brain, we compared the rank of the canonical human match in the rank-ordered similarity profiles between the latent spaces and the original gene expression space (Fig. 4A). The lower the rank, the more similar the canonical pair, with a rank of 1 indicating maximal similarity. We additionally calculated the proportion of latent spaces in which each mouse region was more similar or as similar to its canonical human match compared with the initial gene space (Fig. 4B).

We find that for most regions in this subset, the classification approach either improves the correspondence or performs as well as the full set of homologous genes. For example, 73% of regions exhibit improved similarity in at least 80% of latent spaces. The improvement is most pronounced for regions in the cortical subplate and isocortex. In particular, the visual areas improve from a rank of 32 to an average of 10, though the variance is much higher in this case. Many regions in the sub-cortex do not benefit from the gene expression latent spaces since the initial gene set was already recapitulating the appropriate match with maximal similarity. Apart from the pallidum and the medulla, each of these regions is maximally similar to its canonical match in at least 90% of latent spaces. In such cases, the classification approach performs as well as the original approach. Finally, although many regions in the cerebellum feature some improvement in the latent spaces, the variation in the rank of the standard human pair is often quite large, indicating some instability in the neural network's ability to recover these matches. However, while the rank of the canonical pair varies in different instances of the latent space, the top matches for any given cerebellar region are always cerebellar regions. For instance, when the mouse crus 1 is used as the seed region, the human crus 1 is most often assigned a rank between 6 and 9. However, similar proportions in that range occur for the crus 2 and lobules V, VI and VIIIB, indicating that these cerebellar regions are swapping ranks in the different latent spaces. Thus while cerebellar regions are reliably associated with other cerebellar regions in the gene expression latent spaces, these associations are not stable over multiple training runs.

Together, these results demonstrate that the multi-layer perceptron classification approach improves our ability to resolve finer scale mouse-human neuroanatomical matches within the broadly similar regions obtained using the initial gene expression space. By training a classifier to predict the atlas labels in one species, we were able to generate a new common space that amplified the amount of local signal within broadly similar regions while also improving our ability to recover known mouse-human neuroanatomical pairs.

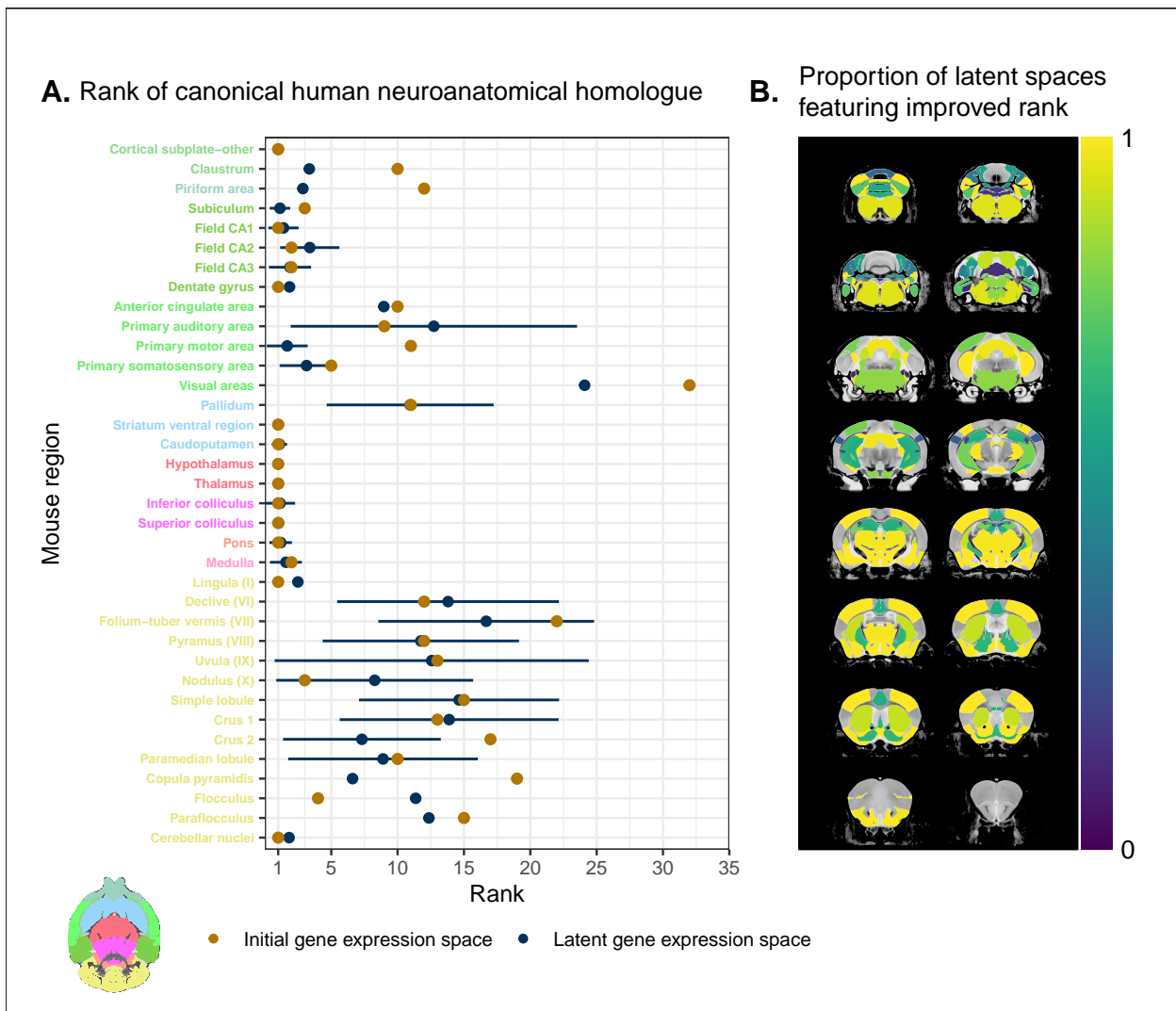


**Fig. 4. Recovering canonical neuroanatomical pairs in gene expression space.** (A) Comparison between the ranks of canonical human matches for mouse seed regions between the initial gene expression space and gene expression latent spaces. Points and error bars represent mean and 95% confidence interval. Mouse region names are coloured according to the AMBA palette. (B) Proportion of latent spaces resulting in an improvement or null difference compared with the initial gene space. Uncoloured voxels correspond to regions with no established canonical human match.

254 **Cortical areas involved in sensorimotor processing show greater transcriptomic**  
255 **similarity than supramodal areas**

256 It is well established that the brains of most, if not all, extant mammalian species follow a common organi-  
257 zational blueprint inherited from an early mammalian ancestor (Kaas, 2011a). A number of cortical subdivi-  
258 sions have consistently been identified in members of many distantly related mammalian species (Krubitzer,  
259 2007) and hypothesized to have been present in the common ancestor of all mammals (Kaas, 2011a). While  
260 it is clear that basic sensorimotor cortical regions are found in the majority of mammals, including mice and  
261 humans, there is much debate about the extent to which cortical areas involved in supramodal processing  
262 are conserved across mammalian taxa. Although some supramodal regions were likely present in the earliest  
263 mammals, including some cingulate regions and an orbitofrontal cortex (Kaas, 2011a), since the divergence  
264 of mouse and human lineages some 80 million years ago, the primate neocortex has undergone substantial  
265 expansion and re-organization (Kaas, 2012). Indeed, when comparing the human neocortex even to primate  
266 model species, this is the likely locus of areas that cannot be easily translated between species (Rogier B.  
267 Mars et al., 2018b). As a result, it is important to investigate whether our between-species mapping is more  
268 successful in somatosensory areas than supramodal areas.

269 We assessed the similarity between mouse and human isocortical areas using the pairwise correlations in each  
270 of the gene expression latent spaces returned from the multi-layer perceptron. For every region in the mouse  
271 isocortex, we evaluated the distribution of maximal correlation values over latent spaces (Fig. 5A). While  
272 the region-wise variance for each isocortical area was large, we found that, on average, sensorimotor regions  
273 exhibited higher maximal correlation values than supramodal regions. The mouse primary somatosensory  
274 and motor areas have the highest average maximal correlation values, with  $r = 0.94 \pm 0.04$  and  $r = 0.93 \pm 0.04$   
275 respectively. We additionally examined the distributions of maximal correlation, grouped by cortex type (Fig.  
276 5B). To generate these distributions, we computed average maximal correlation values by cortex type in each  
277 of the latent spaces. Here too we find that sensorimotor regions are associated with higher maximal  
278 correlation values on average ( $r = 0.89 \pm 0.04$ ), compared with supramodal areas ( $r = 0.85 \pm 0.03$ ). These  
279 distributions demonstrate that sensorimotor isocortical regions exhibit more similarity overall on the basis  
280 of homologous gene expression than do supramodal regions.

281 While we found that sensorimotor isocortical areas in the mouse brain were more similar to human brain  
282 regions than supramodal areas, the distributions of maximal correlation do not speak to the neuroanatomical  
283 patterns of organization for these matches. To understand how the similarity patterns of mouse and human  
284 cortical subdivisions were organized, we used hierarchical clustering to cluster mouse and human isocortical

285 regions on the basis of their similarity profiles in the average gene expression latent space (Fig. 5C). This  
286 allows us to examine the similarity of regions to one another within and across brains at multiple levels  
287 simultaneously.

288 At a high level, we find a striking segregation of the mouse isocortex into one main cluster that corresponds  
289 to regions that are primarily engaged in sensorimotor processing and separate clusters of regions that are  
290 supramodal. All of the sensorimotor areas cluster together, but three supramodal areas also form part of this  
291 cluster: the retrosplenial area, the posterior parietal association areas, and the anterior cingulate cortex. Of  
292 these, the retrosplenial area is the most different, being the first to separate out from the other regions. In  
293 fact, the retrosplenial area is the mouse isocortical region with the smallest correlation values (Fig. 5A). The  
294 mouse sensorimotor cluster is characterized by high correlation values to human sensorimotor regions like  
295 the precentral gyrus, the cuneus, and the postcentral gyrus, as well as low correlation values to the piriform  
296 cortex and paraterminal gyrus.

297 At this level of clustering, the remaining mouse supramodal subdivisions form two clusters. These both  
298 exhibit low similarity to the human somatosensory and visual areas, but the cluster containing the infral-  
299 imbic and perirhinal areas additionally exhibits low correlation values with the precentral gyrus, anterior  
300 paracentral lobule, and transverse gyri. The human cortical regions do not segregate as cleanly into senso-  
301 rimotor and supramodal clusters. Under a similar level of description of four clusters of areas, the majority  
302 of areas belong to a large cluster that includes a mix of cortical types. However, at a lower level of the  
303 hierarchy, if the number of clusters is increased to five, this large cluster breaks up into two smaller clusters  
304 that feature some delineation between supramodal and sensorimotor areas, which are primarily motor and  
305 auditory in nature (e.g. precentral gyrus, Heschl's gyrus). Interestingly, the postcentral gyrus, i.e. primary  
306 somatosensory area, forms a separate cluster with a set of visual areas such as the cuneus and lingual gyrus.  
307 These regions exhibit very similar correlation profiles to the mouse isocortical regions, including maximal  
308 correlation to the mouse primary somatosensory area, with an average of  $r = 0.92$ . The cluster is character-  
309 ized by high correlations to the mouse sensorimotor cluster and low correlations to the mouse supramodal  
310 clusters. Overall the human sensorimotor isocortical regions are loosely organized in clusters that contain  
311 sensory-visual areas and auditory-motor areas.

312 We additionally ran hierarchical clustering on the isocortical similarity matrix in the original homologous  
313 gene space. While the cluster annotations were not substantially different in this space, we observed that  
314 the Euclidean distances within and between clusters were smaller compared with the latent space clustering,  
315 further confirming that the perceptron classification approach improves the segregation of brain regions in  
316 the gene expression common space (Fig. 5D).

317 Overall, we observe a greater degree of similarity between mouse and human cortical regions involved in  
318 basic sensorimotor processing compared with supramodal or association areas. This is in line with the large  
319 body of existing research that suggests that sensory and motor areas of the cortex are conserved across the  
320 brains of mammals. While sensorimotor areas exhibit a greater degree of similarity than supramodal areas,  
321 the neuroanatomical pattern of correspondences obtained using mouse-human homologous genes is not at  
322 the level of individual cortical areas. Still, using a clustering approach we identified clear distinctions in  
323 the patterns of similarity between sensorimotor and supramodal areas, especially for regions in the mouse  
324 isocortex.

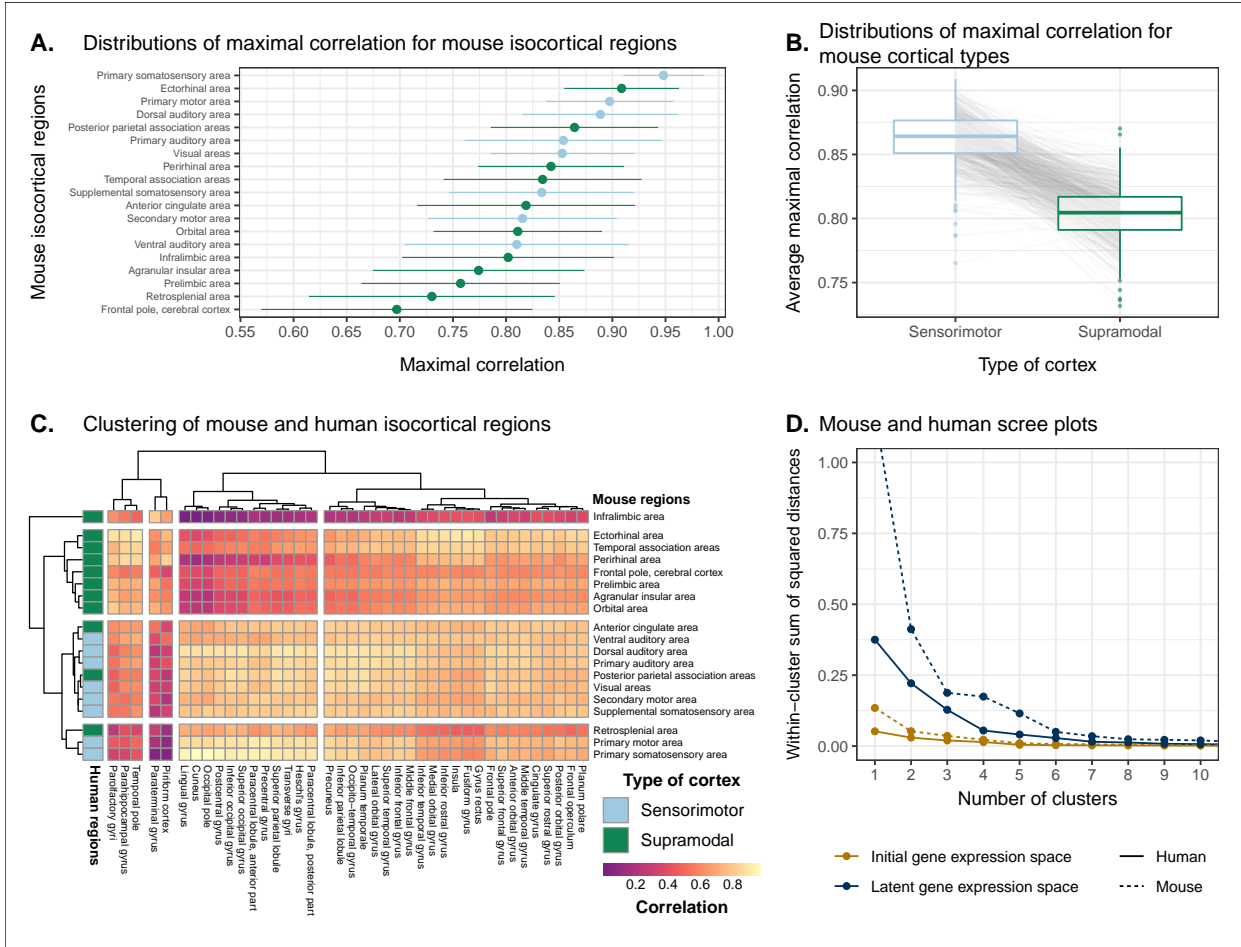


**Fig. 5. Similarity of mouse-human isocortical regions.** (A) Maximal correlation distributions of mouse isocortical regions. Points and error bars represent mean and 95% confidence interval over latent space samples. (B) Distributions of average maximal correlation for sensorimotor and supramodal isocortical areas in each gene expression latent space. Grey lines correspond to individual latent spaces. (C) Hierarchical clustering of mouse and human isocortical regions based on average latent space correlation values. Mouse regions are annotated as sensorimotor or supramodal. Four clusters were chosen for visualization using the elbow method. (D) Within-cluster sum of squared distances for different numbers of mouse and human isocortical clusters in the average latent space and initial homologous gene space.

325 **Transcriptomic comparison of the mouse and human striatum**

326 We have focused here on comparing mouse and human brain organization using transcriptomic data, with  
327 a latent space based on homologous genes as the common space between the two species. To date, common  
328 space comparisons between the mouse and human brain have only been performed using functional con-  
329 nectivity (Balsters et al., 2020; Schaeffer et al., 2020). As a case in point, Balsters et al. (2020) compared  
330 mouse and human striatal organization using this measure. They found that the nucleus accumbens was  
331 highly conserved between mice and humans, and that voxels in the posterior part of the human putamen  
332 were significantly similar to the lateral portion of their mouse caudoputamen parcellation. Additionally,  
333 they report that 85% of voxels in the human striatum were not significantly similar to any of their mouse  
334 striatal seeds, and that 25% of human striatal voxels were significantly dissimilar compared with the mouse.  
335 These differences were understandable, as they involved parts of the human striatum that connected to parts  
336 of prefrontal cortex that have no known homolog in the mouse (Neubert et al., 2014). However, it is not  
337 necessarily the case that between-species differences in connectivity are associated with distinct architectonic  
338 or molecular signatures. Therefore, we investigated the patterns of similarity between the mouse and human  
339 striata on the basis of gene expression using the neural network latent space representations.

340 We first identified the striatal regions present in the Allen human dataset: the caudate, the putamen, and the  
341 nucleus accumbens. We evaluated the correlation between the microarray samples in these regions and every  
342 region in the mouse atlas. Based on these correlation values, we focused our analysis on the four mouse  
343 regions that were consistently the most similar across all latent spaces: the caudoputamen, the nucleus  
344 accumbens, the fundus of striatum, and the olfactory tubercle. For each of the human striatal regions, we  
345 then calculated the average correlation over the samples to each of the mouse targets. We examined the  
346 distribution of these average correlation values over the latent spaces (Fig. 6A). We find that the human  
347 caudate and putamen consistently exhibit the strongest degree of similarity to the mouse caudoputamen.  
348 The median of the distribution for the caudate-caudoputamen pairs is 0.95 and 0.97 for the putamen-  
349 caudoputamen pairs, with modal values of 0.94 and 0.97, respectively. All latent spaces return correlations  
350 greater than 0.9 for caudate-caudoputamen and putamen-caudoputamen pairs. Beyond this expected top  
351 match, the caudate and putamen both exhibit high similarity to the nucleus accumbens and the fundus of  
352 striatum, with mean correlation values of about 0.80. Neither of these target regions is consistently more  
353 similar to the mouse caudoputamen over all latent spaces.

354 While the similarity of the caudate and the putamen to the caudoputamen is unsurprising, the story is not  
355 as clear for the human nucleus accumbens. We find that the variance in correlation calculated over all mouse

356 targets is much lower ( $\sigma = 0.04$ ) compared with the equivalent variances for the caudate ( $\sigma = 0.09$ ) and  
357 putamen ( $\sigma = 0.10$ ), indicating less specificity to any one mouse striatal target. In particular, the human  
358 nucleus accumbens isn't as specifically similar to the mouse nucleus accumbens in the way that the caudate  
359 and putamen are similar to the caudoputamen. The mouse target distributions are right-shifted compared  
360 with those for the caudate and putamen, with mean values of 0.90, 0.89, and 0.89 for the mouse nucleus  
361 accumbens, caudoputamen, and fundus of striatum, respectively. The human accumbens also exhibits a high  
362 degree of similarity to the mouse olfactory tubercle, the distribution of which is also right-shifted compared  
363 with the caudate and putamen.

364 Given the high correlation of the human caudate and putamen to the mouse caudoputamen, as well as the  
365 finding reported by Balsters et al. about the similarity of the lateral caudoputamen to the putamen, we were  
366 curious as to whether we could identify sub-regional patterns of similarity in the caudoputamen and other  
367 striatal regions using these gene expression data. To probe this question, we first examined the average latent  
368 space correlation between each voxel in the mouse striatum and every region in the human atlas. We created  
369 brain maps for the human regions that exhibited the highest mean correlation values, averaged over mouse  
370 striatal voxels: the caudate, the putamen, the nucleus accumbens, and the septal nuclei (Fig. 6B). We find  
371 that voxels in the caudoputamen exhibit a homogeneous pattern of similarity to both the caudate and the  
372 putamen. On average, voxels in the caudoputamen have a correlation of 0.95 to the caudate and 0.94 to the  
373 putamen, with standard deviations of 0.04 and 0.05 respectively. The caudate and putamen are associated  
374 with correlations of at least 0.90 in 88% and 84% of caudoputamen voxels. A number of voxels are also  
375 highly similar to the human nucleus accumbens, with an average correlation value of 0.90 and 55% of voxels  
376 returning a correlation of at least 0.9. The caudoputamen voxels most similar to the nucleus accumbens lie  
377 in the ventral-rostral part of the region. Of course, voxels in the mouse nucleus accumbens are also highly  
378 similar to the human nucleus accumbens, with an average of 0.90 and standard deviation of 0.06. While the  
379 human nucleus accumbens is the most strongly correlated region, a number of voxels also exhibit reasonably  
380 strong correlations to the substantia innominata, the septal nuclei, and the amygdala. Indeed, 91% of voxels  
381 in the accumbens are correlated at a value of 0.7 or higher to the substantia innominata. The equivalent  
382 percentages for the septal nuclei and amygdala are 78% and 74% respectively.

383 We additionally examined the proportion of latent spaces in which each voxel in the mouse striatum was  
384 maximally similar to the human target regions (Fig. 6C). As expected, we find that voxels in the caudop-  
385 utamen are most often maximally similar to the human caudate and putamen, with 75% of voxels in the  
386 caudoputamen being maximally similar to the caudate or putamen in at least 95% of latent spaces, and  
387 62% of voxels being maximally similar to one of those targets in all latent spaces. Interestingly, we observe

388 the emergence of a continuous bilateral pattern of specificity to the caudate and putamen, with voxels in  
389 the rostral and lateral-caudal parts of the caudoputamen being more specific to the caudate, and voxels in  
390 the medial-rostral part being more specific to the putamen. This map highlights subtle differences in the  
391 similarity between caudoputamen voxels and the caudate or putamen. While this pattern distinguishes the  
392 two regions on the basis of which is the top match, individual voxels have very similar correlation values to  
393 the targets (Fig. 6B), with a mean difference in correlation of only 0.006. Beyond the caudoputamen, we  
394 find that the accumbens and olfactory tubercle in the mouse are consistently similar to the human nucleus  
395 accumbens, with 80% of mouse accumbens voxels and 65% of olfactory tubercle voxels having the human  
396 accumbens as their top match in at least 80% of latent spaces. For those voxels below this threshold, the  
397 human regions that are most often the top match are once again the amygdala, the septal nuclei, and the  
398 substantia innominata.

399 Overall, we observe a strong association between the mouse caudoputamen and both the human caudate and  
400 putamen. While we find a subtle pattern of specificity to either region among voxels in the caudoputamen on  
401 the basis of maximal similarity, the high degree of similarity in the correlation values to each region suggests  
402 that the majority of voxels in the caudoputamen are equally similar to the caudate and the putamen on the  
403 basis of the expression of mouse-human homologous genes. We also find that the nucleus accumbens is well  
404 conserved across species. However the region also exhibits patterns of similarity that go beyond the simple  
405 one-to-one match. The human accumbens features similar correlation values to the mouse caudoputamen  
406 and fundus of striatum, in addition to the accumbens proper, with no sharp distinction between these regions.  
407 It also exhibits a larger degree of similarity to the mouse olfactory tubercle. This is also seen in the mouse  
408 striatum, where voxels in the accumbens and the olfactory tubercle map onto the human accumbens.

## 409 Discussion

410 We have demonstrated how spatial transcriptomic patterns of homologous genes can be used to make quan-  
411 titative comparisons between the mouse and human brain. We showed that using homologous genes as a  
412 common space allows one to easily identify coarse similarities in brain structures across species, but that  
413 more fine-scaled parcellations, such as at the level of cortical areas, are more complex. Despite this limi-  
414 tation, the approach still allows for a formal assessment of different patterns of between-species similarity  
415 in primary compared to supramodal regions, identifications of distinct clusters of cortical territories across  
416 species, and comparison of between-species similarities at the transcriptomic level to those observed using  
417 other modalities. We will discuss our observations in the context of the importance of the mouse as a model

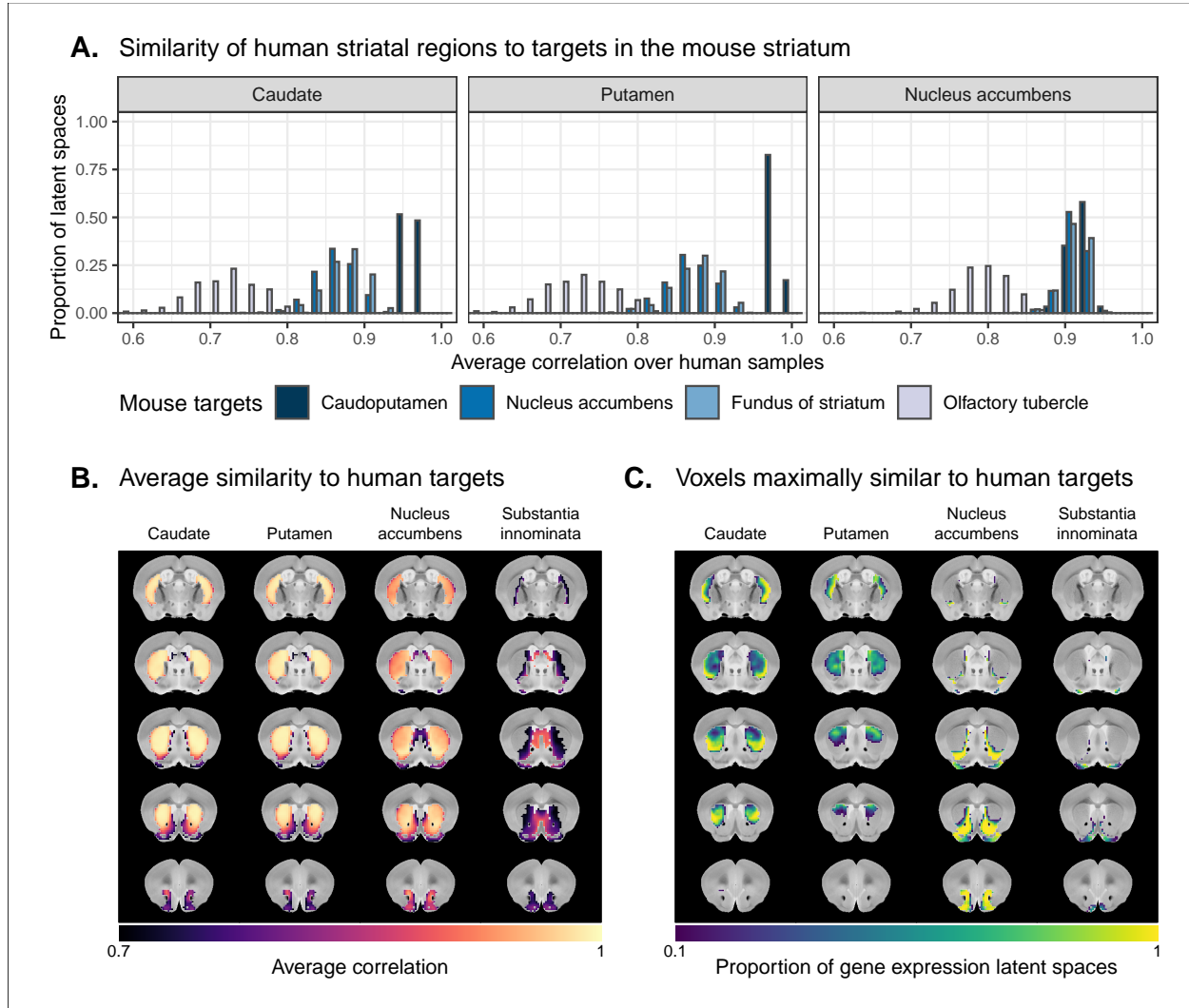


**Fig. 6. Similarity among mouse and human striatal regions.** (A) Distributions over gene expression latent spaces of region-wise average correlation values for mouse and human striatal pairs. Human regions were chosen based on the AHBA ontology. Mouse target regions were chosen to be those with the highest average correlation values. (B) Latent space averaged correlations between voxels in the mouse striatum and human target regions. Target regions were selected based on the highest mean correlation across all striatal voxels. (C) Proportions of latent spaces in which mouse striatal voxels are maximally similar to human target regions.

418 for human neuroscience below.

419 The abundance of neuroscience research performed using mice has resulted in a wealth of knowledge about the  
420 mouse brain. In the preclinical setting, mouse models are utilized with the intention of better understanding  
421 human neuropathology. For instance, in the context of autism spectrum disorders, a plethora of studies  
422 using mouse models have reported on the neurobiological and neuroanatomical phenotypes that arise from  
423 mutations at specific genetic loci (Gompers et al., 2017; Horev et al., 2011; Pagani et al., 2021). It is common  
424 for researchers involved in translational neuroscience to rely on findings of this kind to make inferences about  
425 the human disorder. The typical approach, which is to identify rough post-hoc correspondences between  
426 neuroanatomical ontologies, is not particularly comprehensive and is subject to confirmation bias. While it  
427 may be a reasonable starting point for comparison, the true correspondence between the mouse and human  
428 brain is likely more complicated given the evolutionary distance between the two species. Although overall  
429 patterns of brain organization, including the general pattern of neocortical organization, are similar across  
430 all mammals, substantial differences are evident (Ventura-Antunes et al., 2013). To make matters worse,  
431 researchers from the different neuroscientific traditions often use distinct terminology, further complicating  
432 detailed information exchange. To address these problems, we sought to establish a first quantitative whole-  
433 brain comparison between the two species.

434 The expression of homologous genes provides an elegant way to define a common space for quantitative cross-  
435 species comparisons since it relies on homology at a deep molecular biological level. The approach is not  
436 without limitations however. First, the acquisition of whole-brain transcriptomic data is labour-intensive,  
437 time consuming, and invasive. These data sets cannot be generated easily, especially in the human, in which  
438 the process depends on the availability of post-mortem samples. As a result, the effective sample sizes are  
439 extremely limited in this domain. For instance, in the Allen mouse coronal in-situ hybridization data set  
440 used here, the brain-wide expression of each gene is sampled only once (barring a few exceptions). This  
441 constrains the types of analyses that are possible (e.g. null hypothesis significance testing) and largely limits  
442 the availability of replication data sets. That being said, new technologies, such as spatial transcriptomics,  
443 are gradually making it easier to acquire brain-wide gene expression data in less time and at lower cost (Ortiz  
444 et al., 2020; Stahl et al., 2016; Vickovic et al., 2019). Second, the approach of relying on all available genes  
445 is subject to noise. To address this issue, Myers (2017) (Myers, 2017) used a method of gene set selection  
446 to attempt to improve the correspondence between established mouse-human homologies. While this lead  
447 to improvement, it was only at the level of coarsely defined regions (e.g. cortex-cortex). Our approach,  
448 therefore, was to use supervised machine learning to create a latent common space based on combinations  
449 of homologous genes that can delineate areas within a single species.

450 This latent common space approach led to a substantial improvement in specificity of between-species com-  
451 parisons. Nevertheless, it is evident that the first major distinction in gene expression patterns within a  
452 species, and the easiest identification of similarity across species, is at the coarse anatomical level of the  
453 major subdivisions of the vertebrate brain, such as the isocortex, cerebellar hemispheres and nuclei, and  
454 brain stem. All of these territories were present in the ancestral vertebrate brain (Striedter and Northcutt,  
455 2020) and the ability to detect conserved transcriptomic signatures at this level is not surprising. Within  
456 such structures, such as the isocortex, our ability to make simple one-to-one correspondences decreased. This  
457 is partly because areas within a coarse structure have more similar transcriptomic profiles, but also likely  
458 due to the fact that a single area in one brain does not have a single correspondent in another, larger brain.  
459 In other words, regions in the brains of related species may exhibit one-to-many or many-to-many mappings.  
460 In our study, we found greater cross-species similarity between cortical areas associated with sensorimotor  
461 processing than areas in supramodal cortex. Primary areas, including the sensorimotor areas, are present  
462 in all mammals studied to date and likely part of the common ancestors of all mammals (Kaas, 2011a;  
463 Krubitzer, 2007). Although this common ancestor likely also had non-primary areas, it cannot be denied  
464 that association cortex expanded dramatically in primates and especially so in the human brain (Chaplin et  
465 al., 2013; Mars et al., 2016a). Again, the pattern found here of greater similarity in more conserved areas  
466 might reflect this evolutionary history. In that context it is interesting to note that some non-primary areas  
467 thought to be present in the common mammalian ancestor, such as cingulate and orbitofrontal cortex (Kaas,  
468 2011a) showed relatively high correlation to human areas.

469 An advantage of the approach presented here is that it can, in principle, be applied to any aspect of brain  
470 organization. Beyond simply establishing whether areas are similar across species in a particular common  
471 space, comparing the results across common spaces established using different types of neuronal data can  
472 inform on which larger principles of organization are similar across brains (Eichert et al., 2020). This is  
473 illustrated here by the results of our striatal analysis. We found high similarity between the human caudate  
474 and putamen and mouse caudoputamen, with little differentiation within these regions in a single species.  
475 In contrast, Balsters et al. (2020) demonstrated that human caudoputamen contains a distinct pattern of  
476 connectivity. At first sight, one could argue the results are in contrast. However, evolutionarily speaking, it  
477 is quite probable that an overall similar transcriptomic signature of the striatum can be accompanied by a  
478 distinct connectivity pattern to areas of the cortex present in only one of the two species. Indeed, this speaks  
479 to the different types of similarity that can be studied, depending on which aspect of brain organization one  
480 is interested in. Although the human brain is much larger than the mouse brain and contains a number  
481 of cortical territories that have no homologue in the mouse brain (Kaas, 2011b; Rudebeck and Izquierdo,

482 2022), the similarity in transcriptomic signature mean that translations between the species is valid in many  
483 contexts.

484 The power of a formal understanding of similarities and differences between brains at different levels of  
485 organization is evident. In fundamental neuroscience, it will help translate results from data types that  
486 cannot be obtained in humans to the human brain (Barron et al., 2021). In translational neuroscience, it  
487 will, in a negative sense, help establish the limits of the translational paradigm by showing which aspects  
488 of the human brain cannot be understood using the model species (Liu et al., 2021). In a positive sense,  
489 it will also help by establishing and improving our understanding of the many aspects in which the model  
490 and human brain do concur (Mandino et al., 2021). More ambitious still, it can provide a way in which  
491 highly diverse manifestations of certain disease syndromes (e.g. autism spectrum disorder) (Grzadzinski et  
492 al., 2013; Simonoff et al., 2008) and the availability of many distinct model strains (Ellegood et al., 2015),  
493 each hypothesized to capture a distinct aspect of a multi-dimensional clinical syndrome, can be related to  
494 one another. Ultimately, we believe that using the mapping of homologous gene expression between species  
495 can be an important part of building a transform that maps information obtained using mice to humans and  
496 vice versa.

## 497 Materials and methods

### 498 Mouse gene expression data

499 We used the adult mouse whole-brain in-situ hybridization data sets from the Allen Mouse Brain Atlas  
500 (Lein et al., 2007). Specifically, we used 3D expression grid data, i.e. expression data aligned to the Allen  
501 Mouse Brain Common Coordinate Framework (CCFv3)(Wang et al., 2020) and summarized under a grid  
502 at a resolution of  $200\mu\text{m}$ . We downloaded the gene expression “energy” volumes from both the coronal  
503 and sagittal in-situ hybridization experiments as a sequence of 32-bit float values using the Allen Institute’s  
504 API (<http://help.brain-map.org/display/api/Downloading+3-D+Expression+Grid+Data>). These volumes  
505 were subsequently reshaped into 3D images in the MINC format. Origin, extents, and spacing were defined  
506 such that the image was RAS-oriented, with the origin at the point where the anterior commissure crosses  
507 the midline. The MINC images from the coronal and sagittal data sets were then processed separately  
508 using the Python programming language. The sagittal data set was first filtered to keep only those genes  
509 that were also present in the coronal set. Images were imported using the `pyminc` package, masked and  
510 reshaped to form an experiment-by-voxel expression matrix. We pre-processed this data by first applying a

511 `log2` transformation for consistency with the human data set. For those genes associated with more than  
512 one in-situ hybridization experiment, we averaged the expression of each voxel across the experiments. We  
513 subsequently filtered out genes for which more than 20% of voxels contained missing values. Finally, we  
514 applied a K-nearest neighbours algorithm to impute the remaining missing values. The result of this pre-  
515 processing pipeline was a gene-by-voxel expression matrix with 3958 genes and 61315 voxels for the coronal  
516 data set and a matrix with 3619 genes and 26317 voxels for the sagittal data set.

## 517 Human gene expression data

518 Human gene expression data was obtained from the Allen Human Brain Atlas (Hawrylycz et al., 2012). The  
519 data were downloaded from the Allen Institute’s API (<http://api.brain-map.org>) using the `abagen` package  
520 in Python (<https://abagen.readthedocs.io/en/stable/>) (Markello et al., 2021). We used the microarray data  
521 from the brains of all six donors, each of which contains `log2` expression values for 58692 gene probes  
522 across numerous tissue samples. The data were pre-processed using a custom pipeline built following the  
523 recommendations from Arnatkeviciūtė et al. (Arnatkeviciūtė et al., 2019). The pipeline was implemented  
524 using the R programming language. Specifically, once imported, we passed the data from individual donors  
525 through a set of filters. The first filter removed gene probes that were not associated with an existing Entrez  
526 gene ID. The second filtering step used the probe intensity filter provided by the AHBA. For each donor,  
527 we only retained the probes for which more than 50% of samples passed the intensity filter. After filtering,  
528 we aggregated the expression values for probes that corresponded to the same gene. To do so, we computed  
529 the average expression per sample for probes corresponding to a given gene. This was done separately for  
530 each donor, and the averages were computed in linear space rather than `log2` space. Once the average gene  
531 expression values were obtained, we transformed the data back to `log2` space. Finally, we combined the  
532 gene-by-sample expression matrices across the different donors. In doing so, we retained only those genes  
533 present in the data sets from all six donors. The result was a gene-by-sample expression matrix with 15125  
534 genes and 3702 samples.

## 535 Mouse atlases

536 We used a version of the DSURQE atlas from the Mouse Imaging Centre (Dorr et al., 2008; Qiu et al., 2018;  
537 Richards et al., 2011; Steadman et al., 2014; Ullmann et al., 2013), modified using the AMBA hierarchical  
538 ontology, which was downloaded from the Allen Institute’s API. The labels of the DSURQE atlas correspond  
539 to the leaf node regions in the AMBA ontology, which allowed us to use the hierarchical neuroanatomical

540 tree to aggregate and prune the atlas labels to the desired level of granularity. For the purposes of our  
541 analyses, we removed white matter and ventricular regions entirely. The remaining grey matter regions were  
542 aggregated up the hierarchy so that the majority of resulting labels contained enough voxels to be classified  
543 appropriately by the multi-layer perceptron. In doing so, we maintained approximately the same level of  
544 tree depth within a broad region (e.g. cerebellar regions were chosen at the same level of granularity). This  
545 resulted in a mouse atlas with 67 grey matter regions. We additionally generated an atlas with 11 broader  
546 regions for visualization and annotation purposes.

## 547 Human atlases

548 We used the hierarchical ontology from the AHBA, which we obtained using the Allen Institute’s API.  
549 We aggregated and pruned the neuroanatomical hierarchy to correspond roughly to the level of granularity  
550 obtained in our mouse atlas, resulting in 88 human brain regions. We additionally generated a set of 16  
551 broad regions for visualization and annotation. White matter and ventricular regions were omitted entirely.

## 552 Regional expression and similarity matrices

553 We created the mouse and human gene-by-region expression matrices from the mouse gene-by-voxel and  
554 human gene-by-sample expression matrices. First, we intersected the gene sets in these matrices with a  
555 list of 3331 homologous genes obtained from the NCBI HomoloGene database (NCBI, 2018), resulting in  
556 2624 homologous genes present in both the mouse and human expression matrices. We then annotated  
557 each of the human samples with one of the 88 human atlas regions, and each of the mouse voxels with  
558 one of the 67 mouse atlas regions, discarding white matter and ventricular entries in the process. These  
559 labelled expression matrices were subsequently normalized as follows: For each matrix, we first standardized  
560 every gene across all voxels/samples using a z-scoring procedure. We then centered every voxel/sample  
561 by subtracting the average expression over all homologous genes. Finally, we generated the gene-by-region  
562 expression matrices by averaging the expression of every gene over the voxels/samples corresponding to  
563 each atlas region. Using these expression matrices, we generated the mouse-human similarity matrix by  
564 computing the Pearson correlation coefficient between all pairs of mouse and human regions.

## 565 Multi-layer perceptron classification and latent space

566 To improve the resolution of mouse-human neuroanatomical matches, we performed a supervised learning  
567 approach, wherein we trained a multi-layer perceptron neural network to classify 67 mouse atlas regions

568 from the expression values of 2624 homologous genes. We chose a model architecture in which each layer  
569 of the network was fully connected to previous and subsequent layers. To optimize the hyperparameters,  
570 we implemented an ad hoc cross-validation procedure that took into account the fact that the majority of  
571 genes in the coronal AMBA data set are sampled only once over the entire mouse brain. The procedure  
572 involved a combination of the coronal data set and the sagittal in-situ hybridization data sets. For the  
573 sagittal data set, we used the expression matrix described above. However, we used a modified version  
574 of the coronal expression matrix. This matrix was generated using the pipeline described above with the  
575 following modifications: 1. We applied a *unilateral* brain mask to the coronal images since the sagittal data  
576 is unilateral by construction, and 2. we did not aggregate the expression of multiple in-situ hybridization  
577 experiments for those genes in the coronal set pertaining to more than one experiment. We then filtered  
578 these experiment-by-voxel expression matrices according to the list of mouse-human homologous genes, as  
579 well as the human sample expression matrix. We also annotated the voxels in each of the expression matrices  
580 with one of the 67 regions in the mouse atlas. Our validation procedure then involved iterative construction  
581 of training and validation sets by sampling gene experiments from either the coronal or sagittal matrices: For  
582 every gene in the homologous set, we first determined whether that gene was associated with more than one  
583 experiment in the coronal matrix. If this was the case, we randomly sampled one of those experiments for the  
584 training set and one of the remaining experiments for the validation set. If the gene was associated with only  
585 one experiment in the coronal set, we randomly sampled either the coronal or sagittal experiment for the  
586 training set and the other for the validation set. Once the training and validation sets were generated, they  
587 were normalized using the procedure described above. We then trained the neural network using the training  
588 set and evaluated its performance on the validation set. Given that the construction of the training and  
589 validation sets involved some stochasticity, we repeated this construction, training, and validation procedure  
590 10 times for every combination of hyperparameters.

591 The hyperparameters that we optimized using this method were the number of hidden layers in the network,  
592 the number of hidden units (i.e. neurons) per hidden layer, the dropout rate, and the amount weight decay.  
593 The values we optimized over were as follows. We varied the number of hidden layers between 3 and 5. We  
594 varied the number of hidden units between 100 and 1000 in increments of 100. For the dropout rate, we  
595 examined values of 0, 0.25 and 0.50. For the amount of weight decay, we examined values of  $10^{-6}$  and  $10^{-5}$ .  
596 We found that the best-performing model had 3 hidden layers, 200 neurons per layer, a dropout rate of 0,  
597 and a weight decay value of  $10^{-6}$ . This model returned an average classification accuracy of 0.926 on the  
598 training sets and of 0.526 on the validation sets. Following validation, we used the optimal hyperparameters  
599 to train the network on the full bilateral coronal voxel-wise expression matrix.

600 These models were implemented in Python using PyTorch via the `skorch` library (<https://skorch.readthedocs.io/en/stable/>). For both validation and training, the models were trained over 200 epochs  
601 using a maximum learning rate of  $10^{-5}$ . We used the `AdamW` optimization algorithm (Loshchilov and Hutter,  
602 2019) and `OneCycleLR` learning rate scheduler policy. The activation function used in the forward pass  
603 was the rectified linear unit (ReLU) and the loss function was the negative log-likelihood loss, which is the  
604 default for the `NeuralNetClassifier` class in `skorch`.

606 We used the trained perceptron to generate the latent gene expression space. To extract the appropriate  
607 transformation, we removed the predictive output layer and soft-max transformation from the network  
608 architecture. The resulting architecture returns the 200 hidden units in the third hidden layer as the output  
609 of the network. To create the latent space data representations, we applied this network to the mouse  
610 and human gene-by-region expression matrices, transposed so that the genes were the input variables. The  
611 resulting matrices have 200 columns corresponding to the hidden units and 67 (88) rows corresponding to  
612 the mouse (human) regions. They describe each brain region's weight over the hidden units. To create the  
613 similarity matrix, we calculated the Pearson correlation coefficient between all pairs of mouse and human  
614 regions.

615 Given the stochasticity inherent in training the network (e.g. random weight initialization and stochas-  
616 tic optimization), we repeated the training and transformation process 500 times using the same network  
617 architecture and input data.

## 618 Data and code availability

619 This manuscript, including all figures, was generated programmatically using R Markdown (<https://rmarkdown.rstudio.com>) and LATEX(<https://www.latex-project.org>). The Allen Mouse Brain At-  
620 las and Allen Human Brain Atlas data sets are openly accessible and can be downloaded from the  
621 Allen Institute's API (<http://api.brain-map.org>). All of the code and additional data needed to gen-  
622 erate this analysis, including figures and manuscript, is accessible at <https://github.com/abeaucha/MouseHumanTranscriptomicSimilarity/>.  
624

## 625 Acknowledgments

626 We thank C. Hammill, D.J. Fernandes, E. Anagnostou, B.J. Nieman, and E. Sibille for providing advice  
627 and for interesting conceptual discussions. This study was supported by the Canadian Institutes of Health

628 Research (doctoral funding and foreign study award for A.B.). The Wellcome Centre for Integrative Neu-  
629 roimaging is supported by core funding from the Wellcome Trust (203139/Z/16/Z).

## 630 Competing interests

631 The authors declare that they have no competing interests.

## 632 References

- 633 Arnatkevičiūtė A, Fulcher BD, Fornito A. 2019. A practical guide to linking brain-wide gene expression and  
634 neuroimaging data. *NeuroImage* **189**:353–367. doi:10.1016/j.neuroimage.2019.01.011
- 635 Balsters JH, Zerbi V, Sallet J, Wenderoth N, Mars RB. 2020. Primate homologs of mouse cortico-striatal  
636 circuits. *eLife* **9**:24. doi:10.7554/eLife.53680
- 637 Barron HC, Mars RB, Dupret D, Lerch JP, Sampaio-Baptista C. 2021. Cross-species neuroscience:  
638 Closing the explanatory gap. *Philosophical Transactions of the Royal Society B: Biological Sciences*  
639 **376**:20190633. doi:10.1098/rstb.2019.0633
- 640 Burt JB, Demirtaş M, Eckner WJ, Navejar NM, Ji JL, Martin WJ, Bernacchia A, Anticevic A, Murray JD.  
641 2018. Hierarchy of transcriptomic specialization across human cortex captured by structural neuroimag-  
642 ing topography. *Nature Neuroscience* **21**:1251–1259. doi:10.1038/s41593-018-0195-0
- 643 Chaplin TA, Yu H-H, Soares JGM, Gattass R, Rosa MGP. 2013. A Conserved Pattern of Differen-  
644 tial Expansion of Cortical Areas in Simian Primates. *Journal of Neuroscience* **33**:15120–15125.  
645 doi:10.1523/JNEUROSCI.2909-13.2013
- 646 Dietrich MR, Ankeny RA, Chen PM. 2014. Publication Trends in Model Organism Research. *Genetics*  
647 **198**:787–794. doi:10.1534/genetics.114.169714
- 648 Dorr AE, Lerch JP, Spring S, Kabani N, Henkelman RM. 2008. High resolution three-dimensional brain  
649 atlas using an average magnetic resonance image of 40 adult C57Bl/6J mice. *NeuroImage* **42**:60–69.  
650 doi:10.1016/j.neuroimage.2008.03.037
- 651 Eichert N, Robinson EC, Bryant KL, Jbabdi S, Jenkinson M, Li L, Krug K, Watkins KE, Mars RB. 2020.  
652 Cross-species cortical alignment identifies different types of anatomical reorganization in the primate  
653 temporal lobe. *eLife* **9**:e53232. doi:10.7554/eLife.53232
- 654 Ellegood J, Anagnostou E, Babineau BA, Crawley JN, Lin L, Genestine M, DiCicco-Bloom E, Lai JK, Y,  
655 Foster JA, Peñagarikano O, Geschwind DH, Pacey LK, Hampson DR, Laliberté CL, Mills AA, Tam

- 656 E, Osborne LR, Kouwer M, Espinosa-Becerra F, Xuan Z, Powell CM, Raznahan A, Robins DM, Nakai  
657 N, Nakatani J, Takumi T, Eede MC van, Kerr TM, Muller C, Blakely RD, Veenstra-VanderWeele J,  
658 Henkelman RM, Lerch JP. 2015. Clustering autism: Using neuroanatomical differences in 26 mouse  
659 models to gain insight into the heterogeneity. *Molecular Psychiatry* **20**:118–125. doi:10.1038/mp.2014.98
- 660 Ellenbroek B, Youn J. 2016. Rodent models in neuroscience research: Is it a rat race? *Disease Models &*  
661 *Mechanisms* **9**:1079–1087. doi:10.1242/dmm.026120
- 662 Englund M, James SS, Bottom R, Huffman KJ, Wilson SP, Krubitzer LA. 2021. Comparing cortex-wide  
663 gene expression patterns between species in a common reference frame. doi:10.1101/2021.07.28.454203
- 664 Fulcher BD, Murray JD, Zerbi V, Wang X-J. 2019. Multimodal gradients across mouse cortex. *Proceedings*  
665 *of the National Academy of Sciences* **116**:4689–4695. doi:10.1073/pnas.1814144116
- 666 Gompers AL, Su-Feher L, Ellegood J, Copping NA, Riyadh MA, Stradleigh TW, Pride MC, Schaffler MD,  
667 Wade AA, Catta-Preta R, Zdilar I, Louis S, Kaushik G, Mannion BJ, Plajzer-Frick I, Afzal V, Visel  
668 A, Pennacchio LA, Dickel DE, Lerch JP, Crawley JN, Zarbalis KS, Silverman JL, Nord AS. 2017.  
669 Germline Chd8 haploinsufficiency alters brain development in mouse. *Nature Neuroscience* **20**:1062–  
670 1073. doi:10.1038/nn.4592
- 671 Grzadzinski R, Huerta M, Lord C. 2013. DSM-5 and autism spectrum disorders (ASDs): An opportunity  
672 for identifying ASD subtypes. *Molecular Autism* **4**:12. doi:10.1186/2040-2392-4-12
- 673 Hawrylycz MJ, Lein ES, Guillozet-Bongaarts AL, Shen EH, Ng L, Miller JA, Lagemaat LN van de, Smith  
674 KA, Ebbert A, Riley ZL, Abajian C, Beckmann CF, Bernard A, Bertagnolli D, Boe AF, Cartagena PM,  
675 Chakravarty MM, Chapin M, Chong J, Dalley RA, Daly BD, Dang C, Datta S, Dee N, Dolbeare TA, Faber  
676 V, Feng D, Fowler DR, Goldy J, Gregor BW, Haradon Z, Haynor DR, Hohmann JG, Horvath S, Howard  
677 RE, Jeromin A, Jochim JM, Kinnunen M, Lau C, Lazarz ET, Lee C, Lemon TA, Li L, Li Y, Morris JA,  
678 Overly CC, Parker PD, Parry SE, Reding M, Royall JJ, Schulkin J, Sequeira PA, Slaughterbeck CR, Smith  
679 SC, Sodt AJ, Sunkin SM, Swanson BE, Vawter MP, Williams D, Wohnoutka P, Zielke HR, Geschwind  
680 DH, Hof PR, Smith SM, Koch C, Grant SGN, Jones AR. 2012. An anatomically comprehensive atlas of  
681 the adult human brain transcriptome. *Nature* **489**:391–399. doi:10.1038/nature11405
- 682 Hay M, Thomas DW, Craighead JL, Economides C, Rosenthal J. 2014. Clinical development success rates  
683 for investigational drugs. *Nature Biotechnology* **32**:40–51. doi:10.1038/nbt.2786
- 684 Hedrich HJ, Mossman H, Nicklas W. 2004. Chapter 24: Housing and maintenanceThe Laboratory Mouse.  
685 Elsevier Academic Press. pp. 395–408.
- 686 Heukelum S van, Mars RB, Guthrie M, Buitelaar JK, Beckmann CF, Tiesinga PHE, Vogt BA, Glennon  
687 JC, Havenith MN. 2020. Where is Cingulate Cortex? A Cross-Species View. *Trends in Neurosciences*  
688 **43**:285–299. doi:10.1016/j.tins.2020.03.007

- 689 Hodge RD, Bakken TE, Miller JA, Smith KA, Barkan ER, Graybuck LT, Close JL, Long B, Johansen N,  
690 Penn O, Yao Z, Eggermont J, Höllt T, Levi BP, Shehata SI, Aevermann B, Beller A, Bertagnoli D,  
691 Brouner K, Casper T, Cobbs C, Dalley R, Dee N, Ding S-L, Ellenbogen RG, Fong O, Garren E, Goldy  
692 J, Gwinn RP, Hirschstein D, Keene CD, Keshk M, Ko AL, Lathia K, Mahfouz A, Maltzer Z, McGraw  
693 M, Nguyen TN, Nyhus J, Ojemann JG, Oldre A, Parry S, Reynolds S, Rimorin C, Shapovalova NV,  
694 Somasundaram S, Szafer A, Thomsen ER, Tieu M, Quon G, Scheuermann RH, Yuste R, Sunkin SM,  
695 Lelieveldt B, Feng D, Ng L, Bernard A, Hawrylycz M, Phillips JW, Tasic B, Zeng H, Jones AR, Koch  
696 C, Lein ES. 2019. Conserved cell types with divergent features in human versus mouse cortex. *Nature*  
697 **573**:61–68. doi:10.1038/s41586-019-1506-7
- 698 Horev G, Ellegood J, Lerch JP, Son Y-EE, Muthuswamy L, Vogel H, Krieger AM, Buja A, Henkelman RM,  
699 Wigler M, Mills AA. 2011. Dosage-dependent phenotypes in models of 16p11.2 lesions found in autism.  
700 *Proceedings of the National Academy of Sciences* **108**:17076–17081. doi:10.1073/pnas.1114042108
- 701 Houdebine L-M. 2004. Chapter 6: The mouse as an animal model for human diseasesThe Laboratory Mouse.  
702 Elsevier Academic Press. pp. 97–107.
- 703 Kaas JH. 2012. The evolution of neocortex in primates. *Progress in brain research* **195**:91–102.  
704 doi:10.1016/B978-0-444-53860-4.00005-2
- 705 Kaas JH. 2011a. Reconstructing the Areal Organization of the Neocortex of the First Mammals. *Brain,  
706 Behavior and Evolution* **78**:7–21. doi:10.1159/000327316
- 707 Kaas JH. 2011b. Neocortex in early mammals and its subsequent variations. *Annals of the New York  
708 Academy of Sciences* **1225**:10.1111/j.1749-6632.2011.05981.x. doi:10.1111/j.1749-6632.2011.05981.x
- 709 Krubitzer L. 2007. The Magnificent Compromise: Cortical Field Evolution in Mammals. *Neuron* **56**:201–  
710 208. doi:10.1016/j.neuron.2007.10.002
- 711 Laubach M, Amarante LM, Swanson K, White SR. 2018. What, If Anything, Is Rodent Prefrontal Cortex?  
712 *eneuro* **5**:ENEURO.0315–18.2018. doi:10.1523/ENEURO.0315-18.2018
- 713 Lein ES, Hawrylycz MJ, Ao N, Ayres M, Bensinger A, Bernard A, Boe AF, Boguski MS, Brockway KS,  
714 Byrnes EJ, Chen L, Chen L, Chen T-M, Chi Chin M, Chong J, Crook BE, Czaplinska A, Dang CN,  
715 Datta S, Dee NR, Desaki AL, Desta T, Diep E, Dolbeare TA, Donelan MJ, Dong H-W, Dougherty JG,  
716 Duncan BJ, Ebbert AJ, Eichele G, Estin LK, Faber C, Facer BA, Fields R, Fischer SR, Fliss TP, Frenzley  
717 C, Gates SN, Glattfelder KJ, Halverson KR, Hart MR, Hohmann JG, Howell MP, Jeung DP, Johnson  
718 RA, Karr PT, Kawal R, Kidney JM, Knapik RH, Kuan CL, Lake JH, Laramee AR, Larsen KD, Lau C,  
719 Lemon TA, Liang AJ, Liu Y, Luong LT, Michaels J, Morgan JJ, Morgan RJ, Mortrud MT, Mosqueda  
720 NF, Ng LL, Ng R, Orta GJ, Overly CC, Pak TH, Parry SE, Pathak SD, Pearson OC, Puchalski RB,  
721 Riley ZL, Rockett HR, Rowland SA, Royall JJ, Ruiz MJ, Sarno NR, Schaffnit K, Shapovalova NV,

- 722 Sivisay T, Slaughterbeck CR, Smith SC, Smith KA, Smith BI, Sodt AJ, Stewart NN, Stumpf K-R,  
723 Sunkin SM, Sutram M, Tam A, Teemer CD, Thaller C, Thompson CL, Varnam LR, Visel A, Whitlock  
724 RM, Wohlnoutka PE, Wolkey CK, Wong VY, Wood M, Yaylaoglu MB, Young RC, Youngstrom BL, Feng  
725 Yuan X, Zhang B, Zwingman TA, Jones AR. 2007. Genome-wide atlas of gene expression in the adult  
726 mouse brain. *Nature* **445**:168–176. doi:10.1038/nature05453
- 727 Liu X, Eickhoff SB, Caspers S, Wu J, Genon S, Hoffstaedter F, Mars RB, Sommer IE, Eickhoff CR, Chen  
728 J, Jardri R, Reetz K, Dogan I, Aleman A, Kogler L, Gruber O, Caspers J, Mathys C, Patil KR. 2021.  
729 Functional parcellation of human and macaque striatum reveals human-specific connectivity in the dorsal  
730 caudate. *NeuroImage* **235**:118006. doi:10.1016/j.neuroimage.2021.118006
- 731 Loshchilov I, Hutter F. 2019. Decoupled Weight Decay RegularizationProceedings of the Seventh Interna-  
732 tional Conference on Learning Representations. New Orleans.
- 733 Mandino F, Vrooman RM, Foo HE, Yeow LY, Bolton TAW, Salvan P, Teoh CL, Lee CY, Beauchamp A, Luo  
734 S, Bi R, Zhang J, Lim GHT, Low N, Sallet J, Gigg J, Lerch JP, Mars RB, Olivo M, Fu Y, Grandjean J.  
735 2021. A triple-network organization for the mouse brain. *Molecular Psychiatry* 1–8. doi:10.1038/s41380-  
736 021-01298-5
- 737 Markello RD, Arnatkevičiūtė A, Poline J-B, Fulcher BD, Fornito A. 2021. Standardizing workflows in  
738 imaging transcriptomics with the abagen toolbox. *Biorxiv* 22.
- 739 Mars RB, Jbabdi S, Rushworth MFS. 2021. A Common Space Approach to Comparative Neuroscience.  
740 *Annual Review of Neuroscience* **44**:69–86. doi:10.1146/annurev-neuro-100220-025942
- 741 Mars Rogier B, Passingham RE, Jbabdi S. 2018a. Connectivity Fingerprints: From Areal Descriptions to  
742 Abstract Spaces. *Trends in Cognitive Sciences* **22**:1026–1037. doi:10.1016/j.tics.2018.08.009
- 743 Mars RB, Passingham RE, Neubert F-X, Verhagen L, Sallet J. 2016a. Evolutionary specializations of human  
744 association cortexEvolution of Nervous Systems. Academic Press. pp. 185–205.
- 745 Mars RB, Sallet J, Neubert F-X, Rushworth MFS. 2013. Connectivity profiles reveal the relationship between  
746 brain areas for social cognition in human and monkey temporoparietal cortex. *Proceedings of the National  
747 Academy of Sciences* **110**:10806–10811. doi:10.1073/pnas.1302956110
- 748 Mars Rogier B, Sotiropoulos SN, Passingham RE, Sallet J, Verhagen L, Khrapitchev AA, Sibson N, Jbabdi S.  
749 2018b. Whole brain comparative anatomy using connectivity blueprints. *eLife* **7**. doi:10.7554/eLife.35237
- 750 Mars RB, Verhagen L, Gladwin TE, Neubert F-X, Sallet J, Rushworth MFS. 2016b. Compar-  
751 ing brains by matching connectivity profiles. *Neuroscience & Biobehavioral Reviews* **60**:90–97.  
752 doi:10.1016/j.neubiorev.2015.10.008
- 753 Myers E. 2017. Molecular neuroanatomy: Mouse-human homologies and the landscape of genes implicated  
754 in language disorders (PhD thesis). Boston University.

- 755 NCBI. 2018. Database resources of the National Center for Biotechnology Information. *Nucleic Acids*  
756 *Research* **46**:D8–D13. doi:10.1093/nar/gkx1095
- 757 Neubert F-X, Mars RB, Thomas AG, Sallet J, Rushworth MFS. 2014. Comparison of Human Ventral  
758 Frontal Cortex Areas for Cognitive Control and Language with Areas in Monkey Frontal Cortex. *Neuron*  
759 **81**:700–713. doi:10.1016/j.neuron.2013.11.012
- 760 Oh SW, Harris JA, Ng L, Winslow B, Cain N, Mihalas S, Wang Q, Lau C, Kuan L, Henry AM, Mortrud MT,  
761 Ouellette B, Nguyen TN, Sorensen SA, Slaughterbeck CR, Wakeman W, Li Y, Feng D, Ho A, Nicholas  
762 E, Hirokawa KE, Bohn P, Joines KM, Peng H, Hawrylycz MJ, Phillips JW, Hohmann JG, Wohynoutka  
763 P, Gerfen CR, Koch C, Bernard A, Dang C, Jones AR, Zeng H. 2014. A mesoscale connectome of the  
764 mouse brain. *Nature* **508**:207–214. doi:10.1038/nature13186
- 765 Ortiz C, Fernandez Navarro J, Jurek A, Märtin A, Lundeberg J, Meletis K. 2020. Molecular atlas of the  
766 adult mouse brain. *Science Advances* **6**:14.
- 767 Pagani M, Barsotti N, Bertero A, Trakoshis S, Ulysse L, Locarno A, Miseviciute I, De Felice A, Canella C,  
768 Supek K, Galbusera A, Menon V, Tonini R, Deco G, Lombardo MV, Pasqualetti M, Gozzi A. 2021.  
769 mTOR-related synaptic pathology causes autism spectrum disorder-associated functional hyperconnec-  
770 tivity. *Nature Communications* **12**:6084. doi:10.1038/s41467-021-26131-z
- 771 Passingham RE, Stephan KE, Kötter R. 2002. The anatomical basis of functional localization in the cortex.  
772 *Nature Reviews Neuroscience* **3**:606–616. doi:10.1038/nrn893
- 773 Preuss TM. 1995. Do rats have prefrontal cortex? The Rose-Woolsey-Akert program reconsidered. *Journal*  
774 *of Cognitive Neuroscience* **7**:24.
- 775 Qiu LR, Fernandes DJ, Szulc-Lerch KU, Dazai J, Nieman BJ, Turnbull DH, Foster JA, Palmert MR, Lerch  
776 JP. 2018. Mouse MRI shows brain areas relatively larger in males emerge before those larger in females.  
777 *Nature Communications* **9**:2615. doi:10.1038/s41467-018-04921-2
- 778 Richards K, Watson C, Buckley RF, Kurniawan ND, Yang Z, Keller MD, Beare R, Bartlett PF, Egan  
779 GF, Galloway GJ, Paxinos G, Petrou S, Reutens DC. 2011. Segmentation of the mouse hippocampal  
780 formation in magnetic resonance images. *NeuroImage* **58**:732–740. doi:10.1016/j.neuroimage.2011.06.025
- 781 Rudebeck PH, Izquierdo A. 2022. Foraging with the frontal cortex: A cross-species evaluation of reward-  
782 guided behavior. *Neuropsychopharmacology* **47**:134–146. doi:10.1038/s41386-021-01140-0
- 783 Sallet J, Mars RB, Noonan MP, Neubert F-X, Jbabdi S, O'Reilly JX, Filippini N, Thomas AG, Rushworth  
784 MF. 2013. The Organization of Dorsal Frontal Cortex in Humans and Macaques. *Journal of Neuroscience*  
785 **33**:12255–12274. doi:10.1523/JNEUROSCI.5108-12.2013
- 786 Schaeffer DJ, Hori Y, Gilbert KM, Gati JS, Menon RS, Everling S. 2020. Divergence of rodent and pri-  
787 mate medial frontal cortex functional connectivity. *Proceedings of the National Academy of Sciences*

- 788        117:21681–21689. doi:10.1073/pnas.2003181117
- 789    Simonoff E, Pickles A, Charman T, Chandler S, Loucas T, Baird G. 2008. Psychiatric Disorders in Children  
790        With Autism Spectrum Disorders: Prevalence, Comorbidity, and Associated Factors in a Population-  
791        Derived Sample. *Journal of the American Academy of Child & Adolescent Psychiatry* 47:921–929.  
792        doi:10.1097/CHI.0b013e318179964f
- 793    Stahl PL, Salmén F, Vickovic S, Lundmark A, Navarro JF, Magnusson J, Giacomello S, Asp M, Westholm  
794        JO, Huss M, Mollbrink A, Linnarsson S, Codeluppi S, Borg Å, Pontén F, Costea PI, Sahlén P, Mulder  
795        J, Bergmann O, Lundeberg J, Frisén J. 2016. Visualization and analysis of gene expression in tissue  
796        sections by spatial transcriptomics. *Science* 353:78–82. doi:10.1126/science.aaf2403
- 797    Steadman PE, Ellegood J, Szulc KU, Turnbull DH, Joyner AL, Henkelman RM, Lerch JP. 2014. Genetic  
798        Effects on Cerebellar Structure Across Mouse Models of Autism Using a Magnetic Resonance Imaging  
799        Atlas: MRI of genetic mouse model's cerebellum. *Autism Research* 7:124–137. doi:10.1002/aur.1344
- 800    Striedter GF, Northcutt RG. 2020. Brains Through Time. Oxford University Press.
- 801    Ullmann JFP, Watson C, Janke AL, Kurniawan ND, Reutens DC. 2013. A segmentation protocol and MRI  
802        atlas of the C57BL/6J mouse neocortex. *NeuroImage* 78:196–203. doi:10.1016/j.neuroimage.2013.04.008
- 803    Ventura-Antunes L, Mota B, Herculano-Houzel S. 2013. Different scaling of white matter volume, cor-  
804        tical connectivity, and gyration across rodent and primate brains. *Frontiers in Neuroanatomy* 7.  
805        doi:10.3389/fnana.2013.00003
- 806    Vickovic S, Eraslan G, Salmén F, Klughammer J, Stenbeck L, Schapiro D, Äijö T, Bonneau R, Bergenstråhlé  
807        L, Navarro JF, Gould J, Griffin GK, Borg Å, Ronaghi M, Frisén J, Lundeberg J, Regev A, Ståhl PL.  
808        2019. High-definition spatial transcriptomics for in situ tissue profiling. *Nature methods* 16:987–990.  
809        doi:10.1038/s41592-019-0548-y
- 810    Wang Q, Ding S-L, Li Y, Royall J, Feng D, Lesnar P, Graddis N, Naeemi M, Facer B, Ho A, Dolbeare T,  
811        Blanchard B, Dee N, Wakeman W, Hirokawa KE, Szafer A, Sunkin SM, Oh SW, Bernard A, Phillips  
812        JW, Hawrylycz M, Koch C, Zeng H, Harris JA, Ng L. 2020. The Allen Mouse Brain Common Coordinate  
813        Framework: A 3D Reference Atlas. *Cell* 181:936–953.e20. doi:10.1016/j.cell.2020.04.007
- 814    Yao Z, Velthoven CTJ van, Nguyen TN, Goldy J, Sedeno-Cortes AE, Baftizadeh F, Bertagnolli D, Casper  
815        T, Chiang M, Crichton K, Ding S-L, Fong O, Garren E, Glandon A, Gouwens NW, Gray J, Graybuck  
816        LT, Hawrylycz MJ, Hirschstein D, Kroll M, Lathia K, Lee C, Levi B, McMillen D, Mok S, Pham T,  
817        Ren Q, Rimorin C, Shapovalova N, Sulc J, Sunkin SM, Tieu M, Torkelson A, Tung H, Ward K, Dee N,  
818        Smith KA, Tasic B, Zeng H. 2021. A taxonomy of transcriptomic cell types across the isocortex and  
819        hippocampal formation. *Cell* 184:3222–3241.e26. doi:10.1016/j.cell.2021.04.021